

Dispersion of the superconducting spin resonance in underdoped and antiferromagnetic BaFe_2As_2

D. K. Pratt,¹ A. Kreyssig,¹ S. Nandi,¹ N. Ni,¹ A. Thaler,¹ M. D. Lumsden,² W. Tian,¹ J. L. Zarestky,¹ S. L. Bud'ko,¹ P. C. Canfield,¹ A. I. Goldman,¹ and R. J. McQueeney¹

¹*Department of Physics and Astronomy and Ames Laboratory, Iowa State University, Ames, Iowa 50011, USA*

²*Oak Ridge National Laboratory, Oak Ridge, Tennessee 37831, USA*

(Received 18 February 2010; revised manuscript received 9 April 2010; published 29 April 2010)

Inelastic neutron-scattering measurements have been performed on underdoped $\text{Ba}(\text{Fe}_{1-x}\text{Co}_x)_2\text{As}_2$ ($x=4.7\%$) where superconductivity and long-range antiferromagnetic (AFM) order coexist. The magnetic spectrum found in the normal state is strongly damped and develops into a magnetic resonance feature below T_c that has appreciable dispersion along \mathbf{c} axis with a bandwidth of 3–4 meV. This is in contrast to the optimally doped $x=8.0\%$ composition, with no long-range AFM order, where the resonance exhibits a much weaker dispersion. [see M. D. Lumsden *et al.*, Phys. Rev. Lett. **102**, 107005 (2009).] The results suggest that the resonance dispersion arises from interlayer spin correlations present in the AFM ordered state.

DOI: [10.1103/PhysRevB.81.140510](https://doi.org/10.1103/PhysRevB.81.140510)

PACS number(s): 75.30.Ds, 75.50.Ee, 78.70.Nx, 74.70.Xa

In the recently discovered iron pnictide compounds, magnetism and superconductivity (SC) seem to be intimately linked. SC appears after the antiferromagnetic (AFM) order observed in the parent compound is suppressed.^{1–4} However, the suppression of AFM order need not be complete and both SC and long-range AFM order can coexist in the so-called underdoped (UD) regions of the $\text{Ba}(\text{Fe}_{1-x}\text{Co}_x)_2\text{As}_2$ phase diagram.^{1,4} For these UD compositions, it has been shown that SC and static AFM order are in competition, characterized by a substantial reduction in the AFM order parameter below the superconducting transition temperature (T_c).^{5,6} In addition, inelastic neutron scattering has revealed a resonance in superconducting compositions of $\text{Ba}(\text{Fe}_{1-x}\text{Co}_x)_2\text{As}_2$ below T_c . This resonance appears near the wave vector \mathbf{Q}_{AFM} of the AFM ordered structure.

The resonance has been observed in optimally doped (OD) compositions (defined as having a maximum T_c with no long-range AFM order) (Refs. 7–10) as well as UD compounds with AFM order.^{5,6} For both OD and UD compositions, the resonance is sharply peaked at \mathbf{Q}_{AFM} for momentum in the (\mathbf{ab}) plane (within Fe layers).^{5,6} On the other hand, the energy and intensity of the resonance vary only weakly along the \mathbf{c} axis (perpendicular to the Fe layers) for optimal Co doping⁷ and Ni doping,⁸ suggesting nearly two-dimensional (2D) behavior. Similar to the cuprates,¹¹ the energy of the resonance mode in the OD iron pnictide compounds is in the range of 4–5 $k_B T_c$ and can be associated with the SC gap energy.¹²

In UD compositions, where AFM order persists in the SC state, the effect of the AFM order on the resonance and the relationship between the resonance and spin-wave excitations must also be considered. Here we show that in the UD $\text{Ba}(\text{Fe}_{1-x}\text{Co}_x)_2\text{As}_2$ with $x=4.7\%$ ($T_N=47$ K and $T_c=17$ K) the resonance disperses quite strongly along the \mathbf{c} axis (with an energy window of 4–8 meV), in contrast to the nearly dispersionless resonance found at approximately 9 meV for OD compositions ($x=8\%$ and $T_c=22$ K). This indicates that both the energy and bandwidth of the resonance are composition dependent⁷ and suggests that AFM order leads to the resonance dispersion which bears some similarity to the AFM spin waves themselves.

Inelastic neutron-scattering measurements were performed on the HB3 spectrometer at the High Flux Isotope Reactor at Oak Ridge National Laboratory on single crystals of $\text{Ba}(\text{Fe}_{1-x}\text{Co}_x)_2\text{As}_2$ with $x=4.7\%$. The sample consists of nine coaligned crystals with a total mass of 1.88 g and a total mosaic width of 1.5°. All samples were grown under identical conditions and show the tetragonal-orthorhombic transition of $T_S=60$ K, the Néel transition $T_N=47$ K, and SC transition temperatures at $T_c=17$ K, consistent with crystals used in previous studies.^{2,10} Although the measurements were made below T_S and the sample is orthorhombic, in what follows we describe the scattering vector relative to the high-temperature tetragonal ($I4/mmm$) cell. The sample was aligned in the $(H H L)$ plane and mounted in a closed-cycle refrigerator for low-temperature studies. Measurements were performed with 48'–60'–80'–120' collimation and a fixed final energy of $E_f=14.7$ meV. A pyrolytic graphite (PG) monochromator and analyzer were employed. One PG filter was used after the sample for inelastic measurements while two filters were used for elastic measurements to reduce the signal from higher-order harmonics.

Figure 1 summarizes several features of the neutron intensity $[I(\mathbf{Q}, \omega)]$ above and below T_c in the AFM ordered state. In Fig. 1(a), the energy dependence of the scattering is shown at $T=25$ K above T_c and at $T=5$ K below T_c at $\mathbf{Q}=\mathbf{Q}_{\text{AFM}}=(\frac{1}{2} \frac{1}{2} 1)$. As reported previously,⁵ the data shows a resonance feature at \mathbf{Q}_{AFM} that arises from the redistribution of magnetic intensity from low energies to high energies below T_c . Figure 1(a) also shows estimates of the background $[C(\omega)]$ at both temperatures as obtained from scans at $\mathbf{Q}=(0.35 \ 0.35 \ 1)$ and $(0.65 \ 0.65 \ 1)$ which are far from magnetic intensity centered at \mathbf{Q}_{AFM} and display featureless energy response.

These data can be used to estimate the imaginary part of the magnetic susceptibility at \mathbf{Q}_{AFM} as shown in Fig. 1(b) using the equation

$$\chi''(\mathbf{Q}_{\text{AFM}}, \omega) = [I(\mathbf{Q}_{\text{AFM}}, \omega) - C(\omega)](1 - e^{-\hbar\omega/kT}). \quad (1)$$

The linear energy dependence of the normal-state susceptibility for $\hbar\omega < 6$ meV suggests gapless excitations although

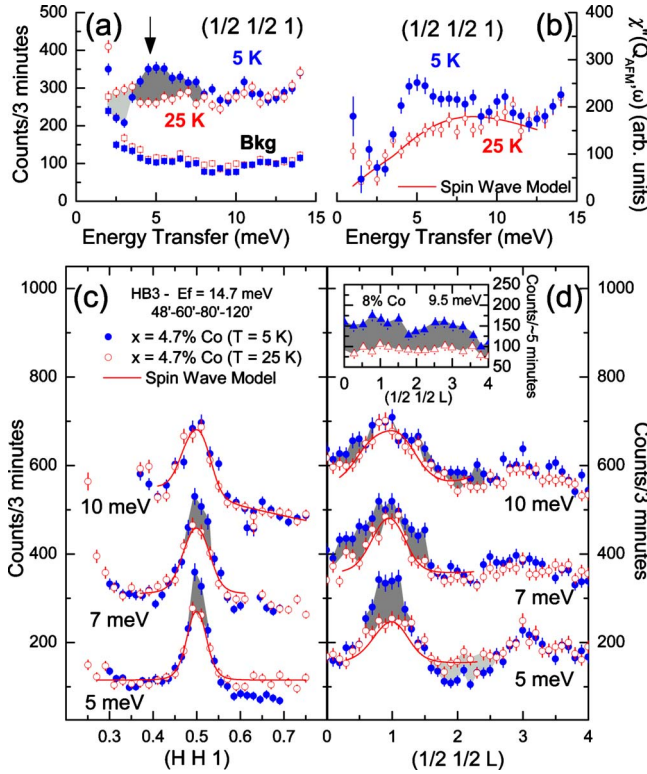


FIG. 1. (Color online) (a) Monitor-normalized neutron intensity $I(\mathbf{Q}, \omega)$ for $x=4.7\%$ including background measurement for energy scans at $\mathbf{Q}_{\text{AFM}}=(\frac{1}{2}, \frac{1}{2}, 1)$ both above (25 K, open circles) and below T_c (5 K, filled circles). The arrow shows the location of the resonance. The dark gray shading highlights regions of increased intensity related to the resonance while the light gray shading highlights a loss of intensity. (b) Energy dependence of $\chi''(\mathbf{Q}_{\text{AFM}}, \omega)$ at 5 and 25 K. The solid line is a fit to spin waves described in the text. (c) $[H H 0]$ scans and (d) $[0 0 L]$ scans through $(\frac{1}{2}, \frac{1}{2}, 1)$ at 5, 7, and 10 meV. In (c) and (d) solid lines represent fits to the spin-wave model in the normal state. The inset in (d) shows $[0 0 L]$ scans for $x=8.0\%$ both above (30 K, open triangles) and below T_c (10 K, filled triangles) at an energy transfer of 9.5 meV (close to the resonance peak) taken from Lumsden *et al.*, Ref. 7.

we cannot ascertain whether a small gap exists below 2 meV due to finite instrumental resolution. A comparison of $\chi''(\mathbf{Q}_{\text{AFM}}, \omega)$ at 25 and 5 K shows that the resonance exhibits an onset at 4 meV, a peak near 5 meV, and a long tail extending up to 10 meV.

Figures 1(c) and 1(d) explore the \mathbf{Q} dependence of the magnetic scattering, showing constant energy scans at 5, 7, and 10 meV along the $[H H 0]$ and $[0 0 L]$ directions through \mathbf{Q}_{AFM} . As expected for the ordered AFM state, the normal-state excitations along $[H H 0]$ are sharply peaked at $(\frac{1}{2}, \frac{1}{2}, 1)$ and appear to be consistent with the steep spin-wave dispersion observed in parent compounds. The normal-state line shapes are much broader along the L direction than in corresponding $[H H 0]$ scans due to the relative weakness of the interlayer exchange. The normal-state spin excitations above T_c were fit using a damped spin-wave model convoluted with the instrumental resolution function [lines in Figs. 1(c) and 1(d)]. The damped spin-wave response function used for analysis is

$$\chi''(\mathbf{q}, \omega) \propto \frac{\Gamma \omega / \hbar}{\hbar^2 (\omega^2 - \omega_{\mathbf{q}}^2 + \Gamma^2 \omega^2)}, \quad (2)$$

$$\hbar \omega_{\mathbf{q}} = \sqrt{v_{ab}^2 (q_x^2 + q_y^2) + v_c^2 q_z^2 + E_g^2}, \quad (3)$$

where v_{ab}/\hbar and v_c/\hbar are the in-plane and interplane spin-wave velocities, E_g is an anisotropy gap, Γ is a damping parameter, and the wave vector \mathbf{q} is defined relative to the magnetic Brillouin-zone center at $\mathbf{Q}_{\text{AFM}}=(\frac{1}{2}, \frac{1}{2}, 1)$. Fits to normal-state spin waves in the $[H H 0]$ and $[0 0 L]$ directions through \mathbf{Q}_{AFM} , shown in Fig. 1, yielded spin-wave velocities of $v_{ab} \geq 123$ meV \AA and $v_c = 43 \pm 9$ meV \AA . The damping and the anisotropy-gap parameters were obtained by fits to both the linear dispersion in Eq. (3) as well as a more general Heisenberg model (not shown) and were found to be in the range of $\Gamma = 8-12$ meV and $E_g = 7-9$ meV. Thus, despite an apparent finite value of the anisotropy gap, spectral weight persists down to the lowest measurable energies due to significant damping [Fig. 1(b)]. However, we note that the damping and anisotropy-gap parameters depend sensitively on estimates of the nonmagnetic background. The fits to a Heisenberg model were generally consistent with the published results for $x=4.0\%$.⁶

Below T_c , Figs. 1(c) and 1(d) show the \mathbf{Q} dependence of the resonance which appears as a change in the intensity of the magnetic scattering below T_c . Similar to other iron pnictides, the SC resonance is sharply defined for wave vectors in the (ab) plane (parallel to the Fe layer) near \mathbf{Q}_{AFM} . The effect of SC on the spin excitations propagating along L is much more interesting. Measurements of the L dependence at the resonance peak energy at 5 meV show that it is narrowly defined at $L=1$, similar to reports for $x=4.0\%$.⁶ At a slightly higher energy of 7 meV, the intensity of the resonance appears to broaden or shift away from $L=1$. At 10 meV, the resonance intensity has weakened considerably and can be found only near the magnetic Brillouin-zone boundary at $L=0$ or 2. This is very different from the L dependence observed in the OD compound with $x=8.0\%$, as determined by Lumsden *et al.* in Ref. 7, where the intensity of the resonance peak (at 10 meV) is broadly distributed along L (Fig. 1, inset).

These results suggest that the resonance observed in UD compositions has dispersion along the L direction. This dispersion is seen more clearly in energy scans measured at $\mathbf{Q}=(\frac{1}{2}, \frac{1}{2}, L)$ for several values of L and temperatures above and below T_c , as shown in Fig. 2(a). As L is increased away from \mathbf{Q}_{AFM} , the resonance intensity shifts to higher energies with L and weakens, being nearly absent at $L=2$. Figure 2(b) compares the difference of intensities measured at 25 and 5 K and $L=0, 1/2$, and 1 as compared to the OD data from Lumsden *et al.* (Ref. 7), illustrating the distinctive behavior of compositions with and without AFM order. Figure 2(c) compares the L dispersion of the resonance peak for UD and OD samples. The UD resonance peak disperses from 5 meV at $\mathbf{Q}_{\text{AFM}}=(\frac{1}{2}, \frac{1}{2}, 1)$ to 8 meV at the zone boundary whereas the resonance of the OD sample remains nearly dispersionless in the range of 8–9 meV.

The resonance dispersion can be fit to an empirical func-

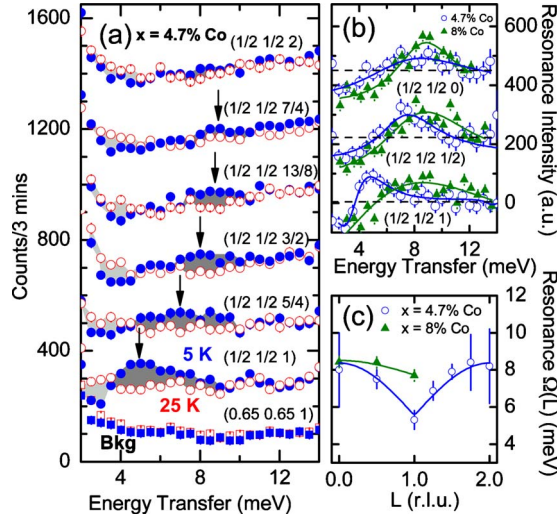


FIG. 2. (Color online) (a) Dispersion of the resonance shown by monitor-normalized constant- \mathbf{Q} energy scans at $(\frac{1}{2}, \frac{1}{2}, L)$ for $x = 4.7\%$ for several values of L at temperatures above and below T_c . (b) Difference of scattering intensity between temperatures 5 K and 25 K above and below T_c , respectively, for both $x = 4.7\%$ (open circles) and 8.0% (filled triangles) at $L = 0, 1/2$, and 1. (c) Comparison of the dispersion of the resonance peak energies along the L direction for $x = 4.7\%$ and 8.0%. The $x = 8.0\%$ data are taken from Ref. 7.

tion $\Omega(L) = \Omega_0 + W|\cos(\pi L/2)|$, where Ω_0 is the energy of the resonance at \mathbf{Q}_{AFM} and W is the bandwidth. For $x = 4.7\%$, $W = 3$ meV, and $W/\Omega_0 = 0.6$, whereas $W/\Omega_0 < 0.1$ for $x = 8.0\%$, as shown in Fig. 2(c). This change in the relative bandwidth with doping suggests that the magnetic resonance is a three-dimensional (3D) feature when AFM and SC co-exist and evolves to a 2D feature upon the loss of magnetic order.

We now discuss the possible origin of the resonance dispersion in the AFM ordered state. The magnetic resonance in iron-pnictide SC has been interpreted in the context of a spin-exciton model^{13,14} where the normal-state spin fluctuations arising from quasiparticle excitations become gapped below T_c . Within the random-phase approximation (RPA), the dynamical magnetic susceptibility in the SC state is given by

$$\chi(\mathbf{Q}, \omega) = \frac{\chi_0(\mathbf{Q}, \omega)}{1 - V(\mathbf{Q})\chi_0(\mathbf{Q}, \omega)}, \quad (4)$$

where $\chi_0(\mathbf{Q}, \omega)$ is the noninteracting dynamical susceptibility in the SC state and $V(\mathbf{Q})$ is an effective spin-spin interaction between itinerant electrons that can be nonlocal.¹² In the SC state, a resonance will appear in $\chi''(\mathbf{Q}, \omega)$ at an energy where $V(\mathbf{Q})\chi_0(\mathbf{Q}, \omega) = 1$. In the pnictides, $\chi_0(\mathbf{Q}, \omega)$ is sharply peaked at $\mathbf{Q} = \mathbf{q}_0 = (1/2, 1/2, 0)$ due to a near nesting of the quasi-2D Fermi surface and the resonance is sharply defined within the (\mathbf{ab}) plane at \mathbf{q}_0 . Along the L direction, the resonance condition is maintained as long as $V(\mathbf{q}_0 + L\hat{z})\chi_0(\mathbf{q}_0 + L\hat{z}, \omega) = 1$, which results in a nearly dispersionless resonance in the quasi-2D limit where both χ_0 and V vary weakly along L . Coherence factors in the SC state cause

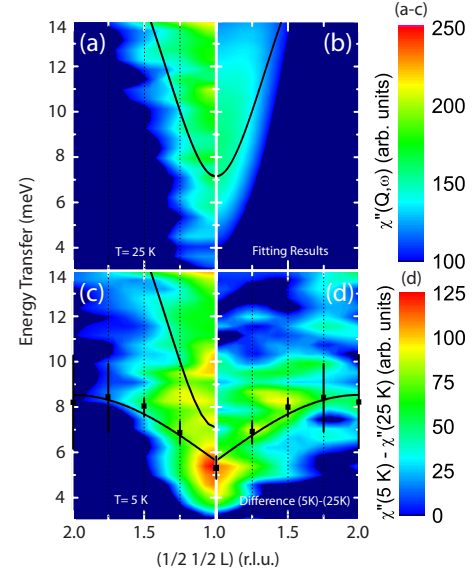


FIG. 3. (Color online) Contour plots of the magnetic susceptibility as a function of $\hbar\omega$ and $L = 1-2$. (a) Measured data at 25 K. The line shows the fitted normal-state spin-wave dispersion. This line also appears in panels (b) and (c). (b) Normal-state damped spin-wave fitting results which have been convoluted with the experimental resolution. (c) Measured data below T_c at 5 K. The lower solid line is a fit to the square data points which represents the peak in the resonance. (d) The measured resonance susceptibility obtained from the difference of the data at 5 K [panel (c)] and 25 K [panel (a)].

a strong enhancement of the resonance intensity when the SC order parameter has sign-reversing symmetry $\Delta_{\mathbf{k}} = -\Delta_{\mathbf{k}+\mathbf{q}_0}$.^{13,14} For an s -wave gap with this property (s^{+-}), the RPA theory predicts that $\Omega_0 \approx 1.4\Delta$ for 2D spin fluctuations at \mathbf{q}_0 . In OD composition, the observed energy and intensity of the resonance and its nearly dispersionless nature appears to support both the quasi-2D spin exciton picture and the s^{+-} symmetry of the SC order parameter.⁷

The presence of 3D AFM order in UD samples requires the introduction of interlayer interactions that result in a stronger L dependence of $V(\mathbf{Q})$ and/or $\chi_0(\mathbf{Q}, \omega)$ due to Fermi-surface reconstruction. The resonance will remain sharply peaked at \mathbf{q}_0 , however, interlayer interactions yield a 3D resonance that is peaked also at $L = 1$, i.e., in the vicinity of the long-range magnetic ordering vector $\mathbf{Q}_{\text{AFM}} = (1/2, 1/2, 1)$. The condition $V(\mathbf{q}_0 + L\hat{z})\chi_0(\mathbf{q}_0 + L\hat{z}, \omega) = 1$ causes dispersion of the resonance along the L direction. As either χ_0 or V are maximum at $L = 1$, the resonance energy will be minimum at \mathbf{Q}_{AFM} and increase along L , with the maximum energy bounded by the SC gap, $\Omega(L) \leq 2\Delta$.^{13,14} Even without long-range AFM order, the presence of pronounced short-range spin correlations along L has been used to explain the weaker resonance dispersion ($W/\Omega_0 = 0.26$) observed in $\text{Ba}(\text{Fe}_{1-x}\text{Ni}_x)_2\text{As}_2$.⁸

Another hallmark of unconventional SC in quasi-2D antiferromagnets is that the ratio $\Omega_0/k_B T_c$ is usually found in the range from 4–5.¹⁵ For $x = 4.7\%$, this ratio is only 3.5, which is somewhat smaller than expected. Even more surprising is that resonance observed in another UD composition with

$x=4.0\%$ ($\Omega_0 \approx 4.5$ meV) (Ref. 6) has a similar energy as $x=4.7\%$. This is true despite the fact that $T_c=11$ K for $x=4.0\%$, whereas $T_c=17$ K for $x=4.7\%$ indicating that there is no scaling between Ω_0 and T_c . It is interesting to note that resonance dispersion is observed in UPd_2Al_3 ($\Omega_0/kT_c=2.8$), where SC also appears within an AFM ordered state ($T_N=17$ K and $T_c=2$ K).^{16,17} CeCoIn_5 is not magnetically ordered, however, strong interlayer spin correlations exist resulting in an L -dependent resonance where $\Omega_0/kT_c=3$.¹⁸

The similar value of Ω_0 in UD 4.0% and 4.7% hints that Ω_0 in AFM ordered systems is influenced by another energy scale, such as the normal-state spin-wave dispersion, anisotropy gap, and/or Landau damping. Figure 3(a) shows a contour plot of the normal-state susceptibility as a function of L and $\hbar\omega$ with the fitted spin-wave dispersion superposed. The zone-boundary spin excitation is estimated to be 20 meV with substantial damping $\Gamma=10$ meV [a calculation of the damped spin-wave susceptibility is shown in Fig. 3(b)]. Figure 3(c) shows the measured susceptibility below T_c with both the resonance and spin-wave dispersion superposed on the image. Figure 3(d) shows the resonance dispersion as the difference of the SC and normal-state susceptibilities. The low-energy spin-wave dispersion along L , combined with large damping, is suggestive of the magnon scenario for the resonance¹⁹ where the SC gap acts to reduce the Landau damping and the subsequent sharpening of spin-wave modes

near or below 2Δ yields a resonancelike feature. The magnon scenario has been used to describe the resonance in the electron-doped cuprates,²⁰ UPd_2Al_3 ,²¹ and CeCoIn_5 .²²

In summary, the weakly dispersive magnetic resonance observed in the superconducting state of OD, paramagnetic, $\text{Ba}(\text{Fe}_{1-x}\text{Co}_x)_2\text{As}_2$ is quasi-2D, but develops significant dispersion along L for UD compositions where AFM and SC coexist (i.e., becomes more 3D). The resonance energy at \mathbf{Q}_{AFM} does not appear to scale with T_c suggesting that the resonance may not have a simple or universal relationship to the SC gap when AFM order exists. The AFM order can be considered as a spin-density wave (SDW) that is stabilized by the gapping of the Fermi surface at \mathbf{Q}_{AFM} and the SDW and SC phases compete as the two gaps vie for the same electrons on the Fermi surface.²³ In this scenario, the interplay of SC and spin excitations, and consequently the resonance, is demonstrably more complex in the presence of AFM order.

The authors would like to thank J. Schmalian, V. P. Antropov, M. R. Norman, R. M. Fernandes, and I. Eremin for valuable comments. Work at the Ames Laboratory is supported by the U.S. Department of Energy Office of Science under Contract No. DE-AC02 07CH11358. Work at Oak Ridge National Laboratory is supported by the Scientific User Facilities Division, Office of Basic Energy Sciences.

- ¹N. Ni, M. E. Tillman, J.-Q. Yan, A. Kracher, S. T. Hannahs, S. L. Bud'ko, and P. C. Canfield, *Phys. Rev. B* **78**, 214515 (2008).
- ²P. C. Canfield, S. L. Bud'ko, Ni Ni, J. Q. Yan, and A. Kracher, *Phys. Rev. B* **80**, 060501(R) (2009).
- ³N. Ni, A. Thaler, A. Kracher, J. Q. Yan, S. L. Bud'ko, and P. C. Canfield, *Phys. Rev. B* **80**, 024511 (2009).
- ⁴J.-H. Chu, J. G. Analytis, C. Kucharczyk, and I. R. Fisher, *Phys. Rev. B* **79**, 014506 (2009).
- ⁵D. K. Pratt, W. Tian, A. Kreyssig, J. L. Zarestky, S. Nandi, N. Ni, S. L. Bud'ko, P. C. Canfield, A. I. Goldman, and R. J. McQueeney, *Phys. Rev. Lett.* **103**, 087001 (2009).
- ⁶A. D. Christianson, M. D. Lumsden, S. E. Nagler, G. J. MacDougall, M. A. McGuire, A. S. Sefat, R. Jin, B. C. Sales, and D. Mandrus, *Phys. Rev. Lett.* **103**, 087002 (2009).
- ⁷M. D. Lumsden, A. D. Christianson, D. Parshall, M. B. Stone, S. E. Nagler, G. J. MacDougall, H. A. Mook, K. Lokshin, T. Egami, D. L. Abernathy, E. A. Goremychkin, R. Osborn, M. A. McGuire, A. S. Sefat, R. Jin, B. C. Sales, and D. Mandrus, *Phys. Rev. Lett.* **102**, 107005 (2009).
- ⁸S. Chi, A. Schneidewind, J. Zhao, L. W. Harriger, L. Li, Y. Luo, G. Cao, Z. Xu, M. Loewenhaupt, J. Hu, and P. Dai, *Phys. Rev. Lett.* **102**, 107006 (2009).
- ⁹S. Li, Y. Chen, S. Chang, J. W. Lynn, L. Li, Y. Luo, G. Cao, Z. Xu, and P. Dai, *Phys. Rev. B* **79**, 174527 (2009).
- ¹⁰D. S. Inosov, J. T. Park, P. Bourges, D. L. Sun, Y. Sidis, A. Schneidewind, K. Hradil, D. Haug, C. T. Lin, B. Keimer, and V. Hinkov, *Nat. Phys.* **6**, 178 (2010).
- ¹¹R. J. Birgeneau, C. Stock, J. M. Tranquada, and K. Yamada, *J. Phys. Soc. Jpn.* **75**, 111003 (2006).
- ¹²M. Eschrig, *Adv. Phys.* **55**, 47 (2006).
- ¹³M. M. Korshunov and I. Eremin, *Phys. Rev. B* **78**, 140509(R) (2008).
- ¹⁴T. A. Maier and D. J. Scalapino, *Phys. Rev. B* **78**, 020514(R) (2008).
- ¹⁵Y. J. Uemura, *Nat. Mater.* **8**, 253 (2009).
- ¹⁶N. Bernhoeft, N. Sato, B. Roessli, N. Aso, A. Hiess, G. H. Lander, Y. Endoh, and T. Komatsubara, *Phys. Rev. Lett.* **81**, 4244 (1998).
- ¹⁷A. Hiess, N. Bernhoeft, N. Metoki, G. H. Lander, B. Roessli, N. K. Sato, N. Aso, Y. Haga, Y. Koike, T. Komatsubara, and Y. Onuki, *J. Phys.: Condens. Matter* **18**, R437 (2006).
- ¹⁸C. Stock, C. Broholm, J. Hudis, H. J. Kang, and C. Petrovic, *Phys. Rev. Lett.* **100**, 087001 (2008).
- ¹⁹A. Chubukov, D. Pines, and J. Schmalian, in *The Physics of Conventional and Unconventional Superconductors*, edited by K. H. Bennemann and J. B. Ketterson (Springer-Verlag, Berlin, 2002), p. 495.
- ²⁰J. P. Ismer, I. Eremin, E. Rossi, and D. K. Morr, *Phys. Rev. Lett.* **99**, 047005 (2007).
- ²¹J. Chang, I. Eremin, P. Thalmeier, and P. Fulde, *Phys. Rev. B* **75**, 024503 (2007).
- ²²A. V. Chubukov and L. P. Gor'kov, *Phys. Rev. Lett.* **101**, 147004 (2008).
- ²³R. M. Fernandes, D. K. Pratt, W. Tian, J. L. Zarestky, A. Kreyssig, S. Nandi, M. G. Kim, A. Thaler, N. Ni, P. C. Canfield, R. J. McQueeney, J. Schmalian, and A. I. Goldman, *Phys. Rev. B* **81**, 140501(R) (2010).